Evaluation and Optimization of an 8-GHz Microwave Electrothermal Thruster

IEPC-2009-201

Presented at the 31st International Electric Propulsion Conference,
University of Michigan • Ann Arbor, Michigan • USA
September 20 – 24, 2009

Jacob H. Blum,[1] Jeffrey R. Hopkins,[2] Michael M. Micci,[3] and Sven G. Bilén[4]
The Pennsylvania State University, University Park, PA 16802, USA

The performance of an 8-GHz microwave electrothermal thruster using ammonia or simulated hydrazine decomposition products as the propellant was measured and optimized by parametrically testing several different configurations. Components that were altered during this testing were antenna depth, propellant, injector size and nozzle size, and material. The configuration that achieved the highest specific impulse, thermal efficiency and thruster efficiency is discussed and considered to be the optimal configuration. This configuration for ammonia propellant consisted of a two-piece chamber separated by a separation plate; an antenna with a flat tip and protruding depth 75% reduced from the baseline configuration; the smallest possible injector diameter without choking the flow; and a stainless steel nozzle with a throat diameter 235% above the baseline diameter. Thermal and thruster efficiencies achieved were improved by 75%, and a 33% improvement in specific impulse above the baseline configuration was achieved. While better results were achieved with the simulated hydrazine propellant than were found in the past, maximum thermal and thruster efficiencies appear to have not been achieved with that propellant.

Nomenclature

γ	=	ratio of specific heats
η_τ	=	thruster efficiency
C_p	=	specific heat (J/kg·K)
CE	=	coupling efficiency
I_{sp}	=	specific impulse (s)
$\dot{m}$	=	mass flow (kg/s)
Pc	=	chamber pressure cold (Pa)
P_h	=	chamber pressure hot (Pa)
P_τ	=	thruster power (W)
P_{abs}	=	absorbed power (W)
P_{for}	=	forward power (W)
P_{input}	=	input power (W)
P_{ref}	=	reflected power (W)
R	=	universal gas constant
T_c	=	chamber temperature cold (K)
T_h	=	chamber temperature hot (K)
u_e	=	exit velocity (m/s)

[1] Graduate Student, Department of Aerospace Engineering, now at Lockheed Martin, jhb177@gmail.com.
[2] Graduate Student, Department of Aerospace Engineering, jrh139@psu.edu.
[3] Professor, Department of Aerospace Engineering, micci@psu.edu.
[4] Associate Professor, Engineering Design, Electrical Engineering, and Aerospace Engineering, sbilen@psu.edu.

I. Introduction

The Microwave Electrothermal Thruster (MET) is a form of electric propulsion that has been under research at The Pennsylvania State University for the past twenty years.[1–14] This device offers several improvements over the arcjet, primarily in performance and material wear. The MET uses microwave energy input into a cavity to set up a resonance mode. This standing wave is used to break down propellant gasses into a coalesced plasma that can be used to heat the propellant gas and then expand it through a nozzle. Penn State has worked on several iterations of this concept spanning frequencies of 2.4, 8, and 14 GHz. This paper focuses on the optimization testing that was performed on the 8-GHz version.

II. Experimental Setup and Testing Procedures

A. Experimental Setup

The 8-GHz MET test apparatus consists of a variety of different components including the propellant control system and its measurement devices; the electromagnetic control system and its measurement devices; and the MET system itself. Each subsystem is discussed separately following Fig. 1, which shows the overall arrangement of the test apparatus. Chamber pressure, vacuum pressure, forward and reflected power, and strain readings are all acquired through LabVIEW data acquisition software. BNC coaxial cables are used to transmit voltage readings from the measurement instruments to a PC running LabVIEW. Microwave frequency and mass flow rates are manually entered into the LabVIEW interface. All of the recorded and inserted values are saved in a spreadsheet for convenient data reduction.

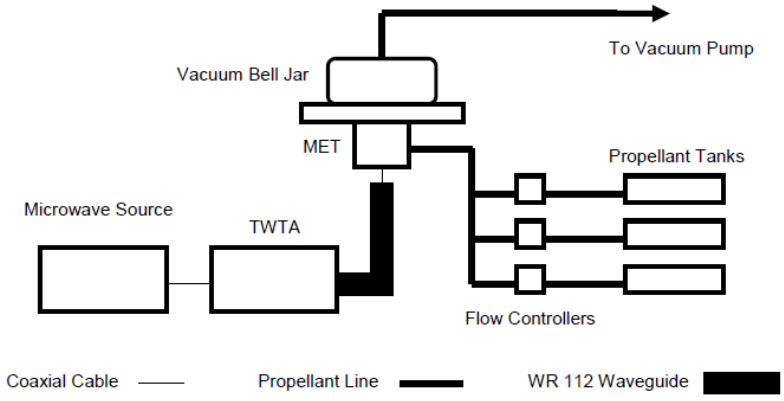

Figure 1. Overall schematic of MET test apparatus.

B. MET System

The MET is constructed from a block of 6061 aluminum alloy. A hole is bored through its center, creating a cylindrical resonance cavity. The dimensions of the cavity were determined to induce a TM^{z}_{011} resonance mode.[4] A quartz window, sealed with an O-ring, is present towards the top of the chamber allowing for viewing of the plasma in the chamber. Two holes are drilled on opposite sides of the chamber, extending tangentially from the circular cavity. This induces the plasma-stabilizing propellant swirl. These holes are created such that a variety of different sized injectors can be interchanged and parametrically tested in the MET. A third hole is drilled perpendicular to the circular cavity allowing for chamber pressure measurements. Four holes located at the corners of the chamber are drilled, allowing for the assembly of the base and nozzle plates with the chamber, as well as attaching the entire assembly to the vacuum flange plate. O-rings are used at the top and bottom of the chamber in order to vacuum seal the contact surfaces of the chamber with the nozzle and base plates, respectively. The only difference being that one chamber has a separation plate positioned on its axial center, separating the antenna from the low pressure plasma. It is vacuum sealed at its contact surfaces using two O-rings.

The base plate of the MET is also made of 6061 aluminum alloy and is sized to match the length and width of the chamber. A small hole is drilled through its center to allow for the insertion of the antenna. The height of the base plate is sized such that the antenna is inserted into the cavity at the optimal electromagnetic resonance depth. An O-ring groove and four small threaded screw holes are drilled into the bottom of the base plate, allowing for the attachment and vacuum sealing of the N-type coaxial panel mount connector which contains the antenna probe.

Many different nozzle plates were parametrically tested to assess the performance variation among them, with a goal of finding the best performing configuration. Six stainless steel converging only nozzle plates and one tungsten converging–diverging nozzle plate, all with different throat diameters, were used in testing.

C. Propellant Control System

Propellant gases are controlled using a number of different sized gas specific flow controllers and transported through a single feed line to the MET. The line is then split and the propellant enters the chamber tangentially on opposite sides of the cavity. The heated propellant is subsequently exhausted through the nozzle, into a vacuum bell jar. A vacuum pump is connected to the bell jar through the same flange plate at which the MET is attached. The propellant flow rates are measured through a multi-gas flow controller and the chamber and vacuum pressures are measured using a pressure transducer and capacitance manometer respectively. Fig. 2 shows a schematic of this system, followed by a list of the various components.

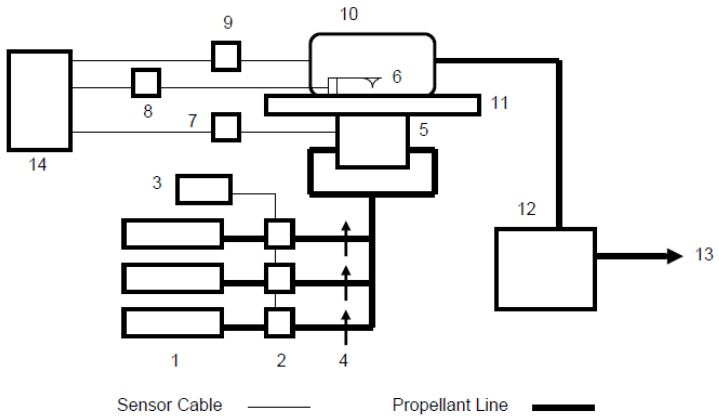

1) Propellant Tanks (NH_3, H_2, N_2)
2) Unit Mass Flow Controllers
   a) UTS-8100 5 SLM N_2
   b) UFC-1660 10 SLM N_2
   c) UFC-8100 1 SLM NH_3
   d) UFC-1660 2 SLM NH_3
   e) UFC-1100A 500 SCCM N_2
3) MKS Multigas Controller 147
4) Propellant Line Ball Valves
5) MET
6) Thrust Stand
7) Omega Pressure Transducer Sensor and Meter
8) Thrust Stand Meter
   a) Instruments Division Wide Range Strain Indicator
   b) Philtec 12V Optical Sensor
9) Hastings Instruments HCM-300 Capacitance Manometer Sensor and Meter
10) Vacuum Bell Jar
11) Vacuum Flange Plate
12) Welch 1402 DuoSeal Vacuum Pump
13) To laboratory ventilation system
14) Chamber pressure, vacuum pressure, and deflection measurement acquisition using LabVIEW installed on Sony Vaio PC

Figure 2. MET propellant control system.

D. Electromagnetic Control system

The electromagnetic control system includes all aspects of the experimental setup pertaining to the control and measurement of the 8-GHz microwave signal through the MET experiment. The signal is created using a HP 8684B 5.4–12.5-GHz signal generator and is connected to an MCL MT3200A traveling wave tube amplifier (TWTA) through an N-type coaxial cable. The TWTA amplifies the signal to the desired power level and transmits it to a series of attached WR112 waveguide sections. The waveguide system is designed to keep reflected power from entering the TWTA in order to avoid damage. After traveling through a series of straight and bent waveguide sections, the signal enters a three-port circulator, which acts as a one way path for the microwave signal. The microwaves enter the circulator through the first port and exit through the second port into a bidirectional waveguide coupler. This section of waveguide has two power connectors attached to its sides, allowing for forward and reflected power measurements using HP and Agilent power sensors. The microwave signal is transitioned from waveguide transmission back to coaxial transmission through a waveguide-to-coaxial transition piece. The signal is finally transmitted into the MET resonant cavity through an N-type panel mount connector with an antenna probe extending into the cavity. TM^z_{011} resonance mode fields are produced in the MET cavity and avalanche ionization of the injected propellants begins, creating a coalesced plasma. Any waves reflected back from the chamber due to a mismatch travel through the bidirectional coupler and are directed into the second port of the three-port circulator. The reflected signal is subsequently directed out of the third port and into a dummy load. These reflected signals are

converted into heat and convected away from the dummy load by cooling fans set up around the experiment. Fig. 3 provides a schematic of this system.

Once the experiment is set up and all of the instruments are turned on, MET performance evaluation and optimization can be conducted. There are two primary testing procedures performed in gathering performance data. The first procedure is the cold flow process. Cold flow values are useful in the evaluation of the MET's performance in a number of ways. Cold flow values are easily measured and are essential in determining the relationship between the Reynolds number and the discharge coefficient. Finally, they aid in calculating the performance of the MET while in operation. Chamber temperatures are not measured during hot fire operation and must be calculated. The pressure values obtained during cold flow and hot fire operation at a given mass flow rate are substituted into their respective mass flow equations in order to obtain a hot and cold temperature ratio. The second testing procedure is the process by which hot fire data is collected.

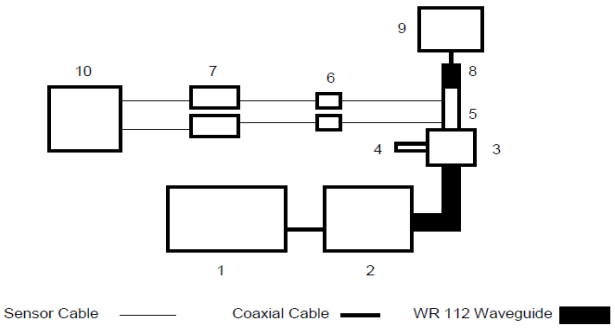

1) HP 8684B 5.4–12.5-GHz Signal Generator
2) MCL MT3200A TWTA, 7.9–8.4-GHz Freq Range, 350 W Max Power
3) Channel Microwave Corp. Three Port Circulator (WR112)
4) ATM WR112 Reflected Signal Dummy Load
5) ATM WR112 Bidirectional Coupler
6) HP and Agilent Power Sensors
7) HP 437B Power Meters
8) WR112 to N-type Coaxial Transition
9) MET
10) Power measurement acquisition using LabVIEW installed on Sony Vaio PC

Figure 3. Electromagnetic control system.

E. Cold Flow Procedure

Before the cold flow procedure can commence, the MET chamber and the bell jar are evacuated by activating the vacuum pump. The lowest vacuum pressure in the bell jar achieved as measured by the capacitance manometer was approximately 0.250 Torr. Once a vacuum is achieved, the desired propellant gas tanks are opened and pressurized. The desired flow rates, controlled by the mass flow controller(s), enter the chamber at fixed increments. When the chamber pressure and vacuum pressure equalize at a given flow rate, the pressure values are recorded by a LabVIEW software application. The incremental value between flow rates is determined by the nozzle's throat diameter and is intended to capture an accurate representation of the thruster's performance at an appropriate resolution. Smaller nozzle throat diameters require smaller increments due to the greater magnitude of the difference in chamber pressures between flow rates. The maximum flow rate reached during cold flow testing is estimated by reviewing the maximum flow rates attained by previous hot fire tests with nozzles of similar throat diameters.

F. Hot Fire Procedure

MET operational testing, also known as hot fire testing, is always conducted directly following a cold flow test. This ensures the least amount of variation between environmental conditions that can alter the results of the tests. Once the signal generator and TWTA are activated, the chamber is evacuated to a pressure in which electrical breakdown can be initiated. This pressure can be less than or equal to approximately 0.50 psia. The input power is subsequently increased to approximately 100 W, igniting a diffuse plasma in the chamber. The propellant flow rate and input power are simultaneously increased to the desired respective starting values. Once these values are achieved, the TWTA is commanded to hold the input power level constant and hot fire data recording can begin. The flow rate values and fixed increment value used for each hot fire test are the same values used for the preceding cold flow test. This allows for the simplest method of pressure ratio calculation. The microwave signal frequency is adjusted at each flow rate in order to obtain the highest coupling efficiency (P_{abs}/P_{for}) possible. The chamber and vacuum pressures are allowed to equilibrate and are subsequently recorded along with the various power readings using LabVIEW. Hot fire testing is completed when the flow controller reaches its maximum flow rate, the performance of the thruster has been visibly declining for a significant amount of preceding flow rates, or the plasma is extinguished.

III. Experimental Results

Optimization testing was performed to obtain an optimized set of parameters for the operation of the MET while at power levels between 100–350 W. Parameters that were investigated were antenna depth, injector diameter, nozzle material, throat diameter, and propellant gas.

G. Nitrogen Gas Propellant Testing Results

The MET chamber was originally designed with a dielectric separation plate located in the center of the cavity.[3] The purpose of this separation plate is to isolate the antenna from the propellant gases that could cause the formation of a plasma at the base of the chamber. This plasma could potentially damage the antenna. However, this separation plate, typically made of brittle materials such as quartz, boron nitride, or a similar ceramic, has a probability of shattering during launch or shock separation events. One of the motivations of the design of this new 8-GHz MET was to create a chamber without a separation plate in order to avoid this potential problem. This chamber was fabricated from a single piece of aluminum. The antenna is insulated from any plasma located at the base of the chamber with a dielectric antenna cap made from either Teflon or Fluoroloy. Preliminary hot fire testing of the 8-GHz MET without a separation plate was conducted using nitrogen and simulated hydrazine.

The nitrogen testing produced a coalesced plasma similar to that produced with the 2.45-GHz and 7.5-GHz MET chambers. Results were obtained and reported in Ref. 4 using this thruster configuration; however, the dielectric cap would periodically ablate because of the formation of a plasma at the base of the chamber, causing damage to the antenna. The ablation of the antenna caps continued in tests performed during the timeframe of the work reported in this paper.

This problem prompted the decision to design a new 8-GHz MET chamber containing a dielectric separation plate. All other aspects of this new chamber are identical to the original one-piece 8-GHz MET chamber. Note that a dielectric antenna cap becomes unnecessary with the addition of a separation plate. Testing of the new chamber was conducted in order to compare performance results with that of the one-piece chamber. Similar results correspond to similar behavior and allow for further optimization of the MET. The parameter used to compare the two chambers is the ratio of hot fire chamber pressure to cold flow chamber pressure at a given flow rate. This ratio is an indication of the chamber temperature and, therefore, I_{sp} performance of the MET. The relationship between pressure and temperature is governed by the equation[15]

$$\frac{T_h}{T_c} = \left(\frac{P_h}{P_c}\right)^2 \left[\frac{\gamma_h \left(\frac{2}{\gamma_h + 1}\right)^{(\gamma_h+1)/(\gamma_h-1)}}{\gamma_c \left(\frac{2}{\gamma_c + 1}\right)^{(\gamma_c+1)/(\gamma_c-1)}}\right], \tag{1}$$

where γ is the ratio of specific heats for the propellant gasses at temperature. Since calculated temperatures did not approach the dissociation temperatures for any of the propellant gasses used, we were able to drop the γ terms and just do a temperature calculation based upon the ratio relationship for pressure and temperature directly. These tests were conducted using nitrogen gas as the propellant. The results of this test are shown in Fig. 4.

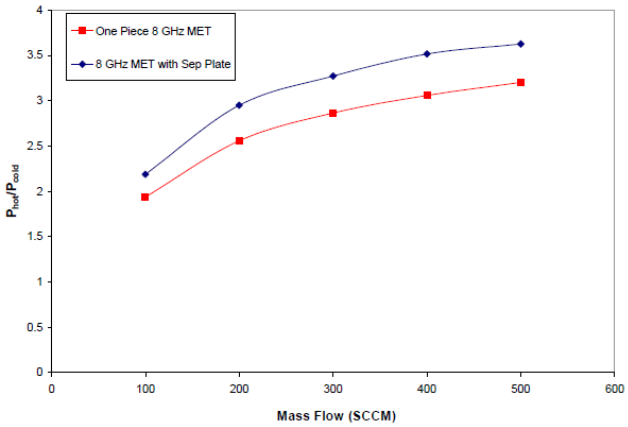

Figure 4. Comparison of the one piece MET with the MET with a separation plate using nitrogen propellant.

H. Ammonia Propellant Results

The 8-GHz MET was parametrically optimized using ammonia gas as the propellant. Ammonia gas is an ideal propellant for the MET for various reasons. The ammonia molecule is lightweight, it dissociates at relatively low temperatures, and ammonia is liquid storable. It should be noted that, in this section and the simulated hydrazine results section, both chamber pressure values and specific power values (P_{for}/m) are normalized to a baseline testing configuration. All of the performance evaluation values, however, are absolute. Before flow-related parameterization can begin, the

electromagnetic fields created in the cavity must be optimized to ensure maximum absorption of the microwave energy by the propellant. Field optimization is achieved by varying the shape of the antenna tip and the antenna's depth into the chamber. The antenna protrudes into the chamber at a certain baseline depth configuration. The antenna's protrusion into the chamber is reduced by the amount presented (50%, 75%, and 88%) for each subsequent antenna configuration. As with the nitrogen hot fire test, pressure ratios calculated for each antenna variation are used to determine performance. Fig. 5 displays the antenna optimization results where two different tip shapes, rounded and flat, at various depths were considered.

The optimal antenna configuration is the 75% reduced depth with a flat tip. It should be noted that although the 50% reduced depth antenna with a round tip outperformed the 50% reduced depth antenna with a flat tip, the implementation of a 75% reduced depth antenna with a round tip was disadvantageous. A section of the rounded tip of this antenna would have been beneath the bottom surface of the cavity, creating variations in the generated electromagnetic field.

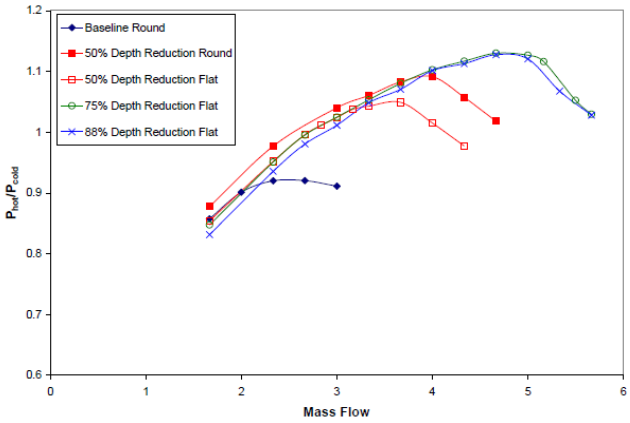

Figure 5. Normalized comparison of pressure ratios for various antenna depths and shapes using ammonia propellant.

I. Flow Related Optimization

The function of the propellant injectors is to regulate the influx of mass flow and swirl behavior. This is accomplished by varying the injector diameter. A smaller diameter results in a higher flow velocity for the same mass flow rate, which in turn produces a tighter plasma stabilizing propellant swirl. The optimized configuration is based on three performance values calculated using the chamber pressures, input powers, and reflected powers collected during testing. The first performance value is the coupling efficiency, which is a measure of the power absorbed by the plasma. This is calculated using the forward and reflected power measurements,

$$CE = \frac{P_{\text{for}} - P_{\text{ref}}}{P_{\text{for}}} = \frac{P_{\text{abs}}}{P_{\text{for}}}. \tag{2}$$

The second value calculated for performance evaluation is the thermal efficiency

$$\eta_t = \frac{\Delta C_p T_c \dot{m}}{P_{\text{for}}}, \tag{3}$$

which is the ratio of propellant specific enthalpy to specific forward power. This value is a measure of the amount of power that is directly used to increase the chamber temperature.

The third value calculated for performance evaluation is the specific impulse, I_{sp}, of the thruster. The pressure values obtained during cold flow and hot fire operation at a given mass flow rate are substituted into their respective mass flow equations in order to obtain a hot and cold temperature ratio listed above. Known pressure and temperature dependant chemical equilibrium constants obtained from sources such as the NASA Glenn Chemical Equilibrium Program are solved simultaneously with the temperature ratio equation to produce a hot fire chamber temperature. This chamber temperature is substituted into the following equation to calculate the exit velocity as

$$u_e = \sqrt{\frac{2\gamma R}{(\gamma - 1)} T_c \left[1 - \left\{ \frac{p_e}{p_c} \right\}^{\frac{\gamma - 1}{\gamma}} \right]}. \tag{4}$$

This exit velocity, in turn, can be used to ultimately calculate the I_{sp} of the thruster. All of these performance evaluation values (coupling efficiency, thermal efficiency, and specific impulse) are plotted against the chamber pressure normalized to a baseline configuration.

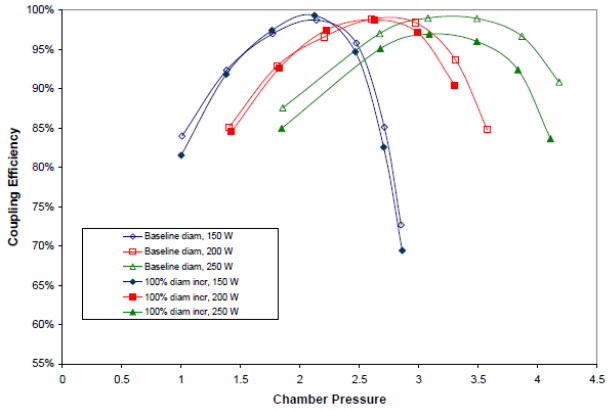

Figure 6. Coupling efficiency vs. normalized chamber pressure comparison of injectors with a baseline diameter and a 100% increase of the baseline diameter at 150, 200, and 250 W using ammonia.

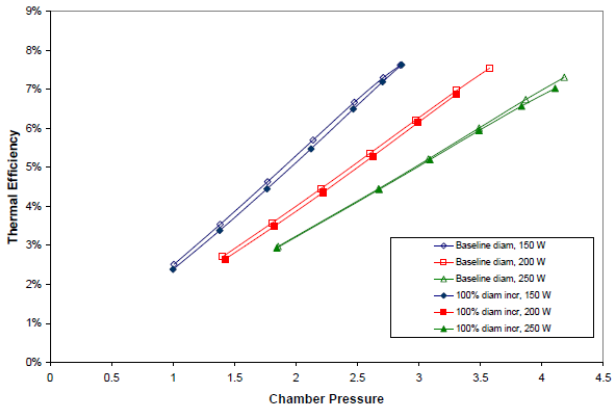

Figure 7. Thermal efficiency vs. normailzed chamber pressure of injectors with baseline diameter and 100% increase of the baseline diameter at 150, 200, and 250 W using ammonia.

The propellant injector optimization consists of two series of tests using different pairs of injectors. Each series tests the chamber conditions at three fixed power levels (150, 200, and 250 W). The diameter of the injectors in the second series of tests are double that of the injectors in the first series of tests. The effects of this variation can be seen in Figs. 6–8.

The data show that the maximum coupling efficiency is not greatly affected by injector diameter. In fact, the maximum coupling efficiency increases at 150 W for a larger injector diameter, remains constant at 200 W, and decreases at 250 W for a larger injector diameter. The thermal efficiency essentially remains unchanged when the injector diameter is increased for all power levels. The only relatively noticeable performance change is specific impulse, which decreases as injector diameter is increased. However, a maximum exit velocity of the injector is reached when the injector is choked. At a constant upstream stagnation pressure (bottle pressure), the choked flow rate decreases for smaller injector diameters and, therefore, places a smaller limit on the maximum flow rate allowed through the injector. Increased mass flow in future tests prohibits the use of injectors with small diameters and therefore low choked flow rates because back pressures cannot be increased above the maximum pressure specifications of the flow controllers. Therefore, the optimal injector diameter is the smallest diameter that does not choke the flow at a given bottle pressure.

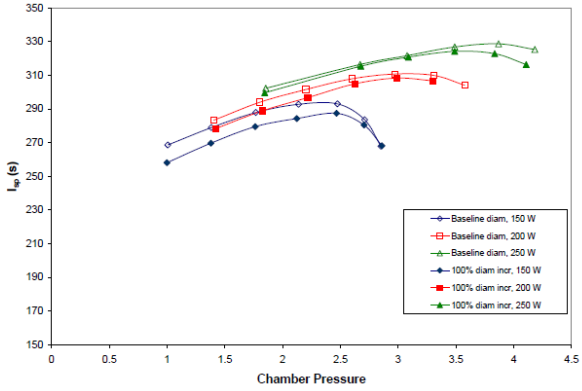

Figure 8. Specific impulse vs. normalized chamber pressure comparison of injectors with a baseline diameter and a 100% increase of the baseline diameter at 150, 200, and 250 W using ammonia.

J. Nozzle Optimization

The second flow control component of the MET is the nozzle. The nozzle regulates the flow exiting the chamber. The nozzle is parameterized by the diameter of the nozzle throat and the material from which it is constructed. The nozzles used for performance optimization of the MET are all made from stainless steel, save that one made from tungsten. The throat diameters of the nozzles incrementally increase from small to large, beginning with a baseline diameter and increasing by 20%, 72%, 150%, 200%, and 235%. The values calculated for performance evaluation and ultimate optimization include the same values used for the injector optimization, these being coupling efficiency, thermal efficiency, and specific impulse. Thruster efficiency is also calculated using

$$\eta_\tau = \frac{P_\tau}{P_{\text{input}}} = \frac{\frac{1}{2}\dot{m}u_e^2}{P_{\text{input}}} \tag{5}$$

in order to provide the overall efficiency of the MET. These four values are plotted against both normalized chamber pressure and normalized specific power. The results shown in Figs. 9–16 depict a series of tests in which each test consists of a constant nozzle throat diameter that is exposed to at least three fixed forward power levels (150, 200, and 250 W). Two additional high power tests (300 and 350 W) were performed on the highest performing nozzles in order to observe increases in the performance of the nozzle.

All of the nozzles attain approximately the same maximum coupling efficiency, regardless of the input power, specific power, or chamber pressure. However, as the input power is increased, the maximum coupling efficiency occurs at higher chamber pressures for all nozzle configurations. This finding implies that an increase in power requires an increase in chamber pressure and, therefore, flow rate to maintain the maximum coupling efficiency of the thruster configuration.

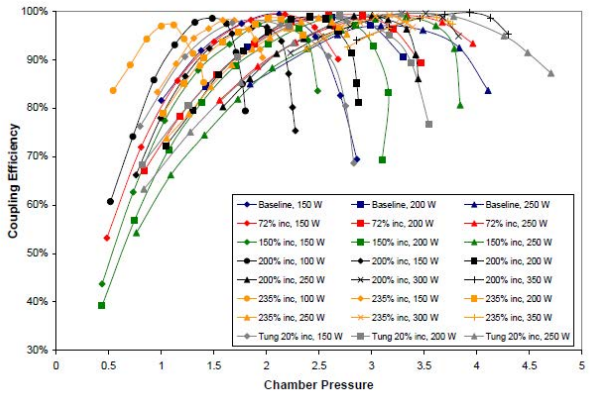

Figure 9. Coupling efficiency vs. normalized chamber pressure for various nozzles.

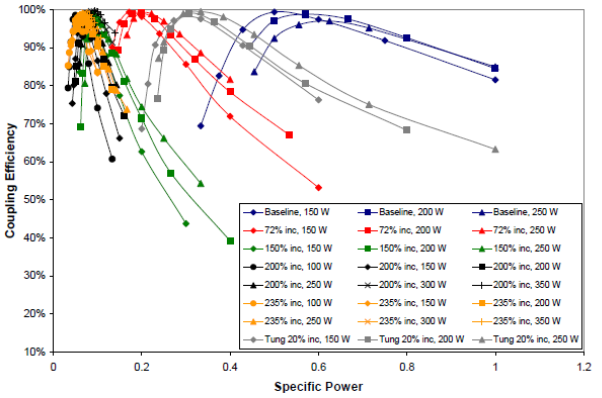

Figure 10. Coupling efficiency vs. normalized specific power for various nozzles using ammonia propellant.

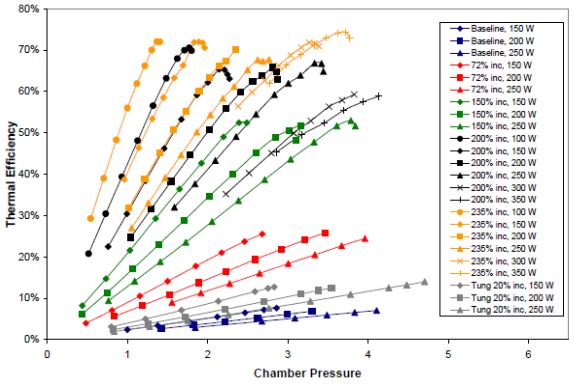

Figure 11. Thermal efficiency vs. normalize chamber pressure for various nozzles using ammonia propellant.

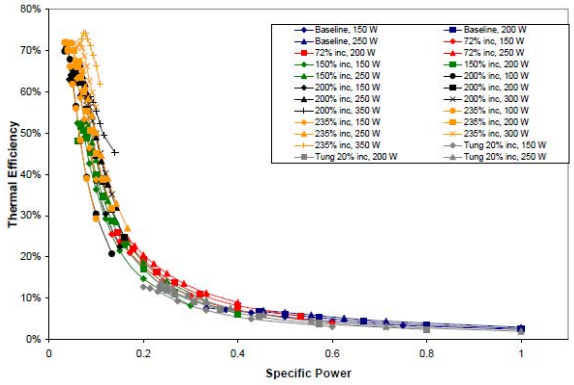

Figure 12. Thermal efficiency vs. normalized specific power for various nozzles using ammonia propellant.

The thermal efficiency increases with chamber pressure and, in turn, increasing mass flow. This is not only evident within each test, but throughout the entire nozzle comparison. Larger nozzles that require higher flow rates have significantly better thermal efficiencies than smaller nozzles with lower flow rates. This finding is reinforced by the fact that lower specific powers result in higher thermal efficiencies. The observation that the input power level does not have a large effect on the thermal efficiency of the configuration implies that thermal efficiencies are dependent mostly on specific powers, instead of absolute power. One interesting note about the thermal efficiency data is that the maximum thermal efficiency does not correspond to the maximum coupling efficiency, but instead occurs at higher chamber pressures. This is more proof that an increase in thermal efficiency is directly related to a decrease in specific power, no matter the amount of absorbed power. Another interesting note about the thermal efficiency data is that the configuration using the tungsten nozzle does not produce thermal efficiencies as high as a stainless steel nozzle of similar throat diameter. This can be attributed to the fact that tungsten has a larger thermal

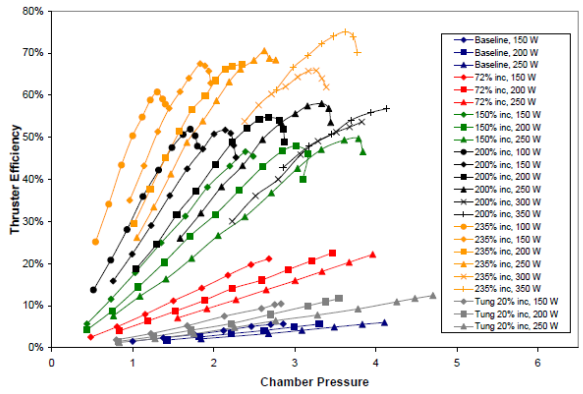

Figure 13. Thruster efficiency vs. normalized chamber pressure for various nozzles using ammonia propellant.

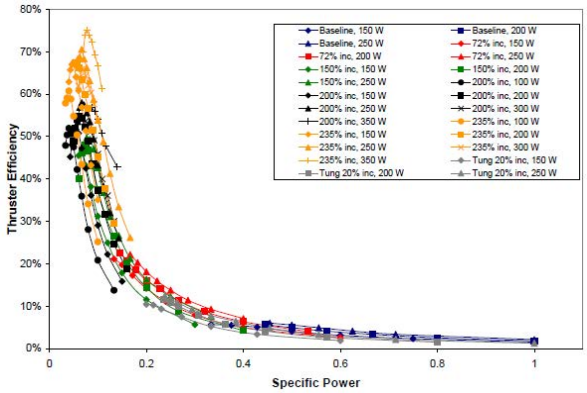

Figure 14. Thruster efficiency vs. normalized specific power for various nozzles using ammonia propellant.

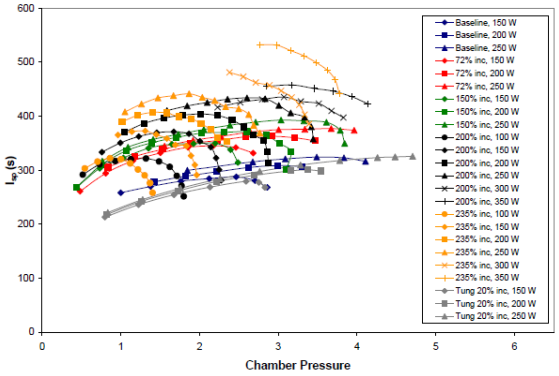

Figure 15. Specific impulse vs. normalized chamber pressure for various nozzles using ammonia propellant.

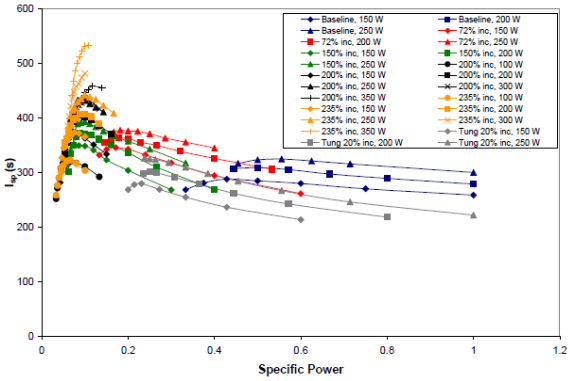

Figure 16. Specific impulse vs. normalized specific power for various nozzles using ammonia propellant.

conductivity value than steel and, in turn, conducts more heat out of the system. The optimized nozzle configuration with regard to thermal efficiency seems to have reached its maximum based on similar results from the two largest nozzles.

Conclusions reached from the thermal efficiency data are echoed by the thruster efficiency data. That is, that specific power is the driving force behind thruster efficiency. However, it should be noted that, although the optimal nozzle configuration seems to have been reached in the case of thermal efficiency, this is not the case with regard to thruster efficiency. The largest nozzle, 235% throat diameter increase from baseline, has significantly higher thruster efficiencies than the second largest nozzle, 200% throat diameter increase from baseline. The data shows that higher thruster efficiencies can still possibly be attained using nozzles with larger throat diameters.

The data show that specific impulse increases with input power. The specific impulse also increases with increasing chamber pressure and decreasing specific power (i.e., increasing mass flow); however, this trend only occurs up to a certain chamber pressure and specific power. It is interesting to observe that this highest performing pressure location occurs at different points depending on the nozzle configuration and, therefore, flow rate. However, the specific power values corresponding to these pressures are all relatively equal. This finding implies that there exists a minimum specific power value at which specific impulse is optimized. The largest nozzle configuration tested, the 235% throat diameter increase from baseline, seems to have reached that optimal minimum specific power. However, increasing input power still significantly improves specific impulse, no matter the specific power value. It should be noted that the tungsten nozzle has the lowest specific impulse observed. Again, this can be attributed to the fact that its thermal conductivity is higher than that of stainless steel.

The optimal nozzle configuration tested with regard to all four performance values is the largest nozzle, the 235% throat diameter increase from baseline. However, higher input power will most assuredly increase the specific impulse and, possibly, the thruster efficiency, which does not appear to have reached a maximum.

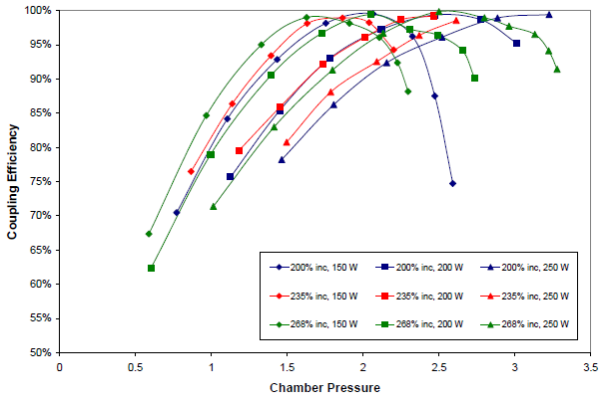

Figure 17. Coupling efficiency vs. normalized chamber pressure for various nozzles using 50% cold decomposed hydrazine.

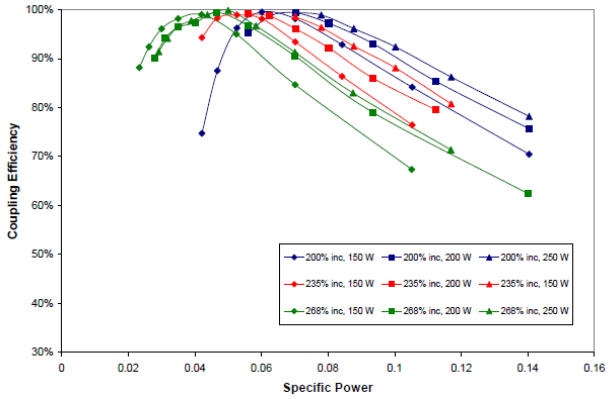

Figure 18. Coupling efficiency vs. normalized specific power for various nozzles using 50% cold decomposed hydrazine propellant.

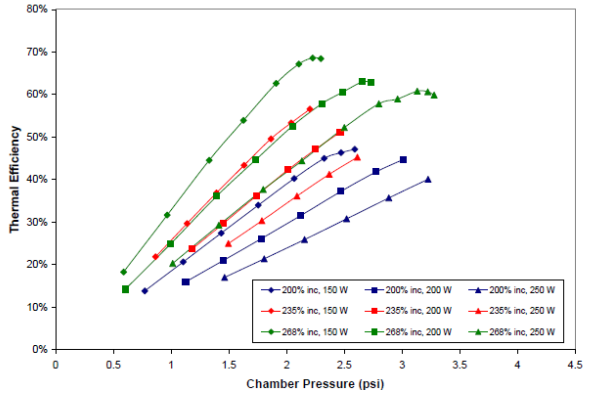

Figure 19. Thermal efficiency vs. normalized chamber pressure for various nozzles using 50% cold decomposed hydrazine.

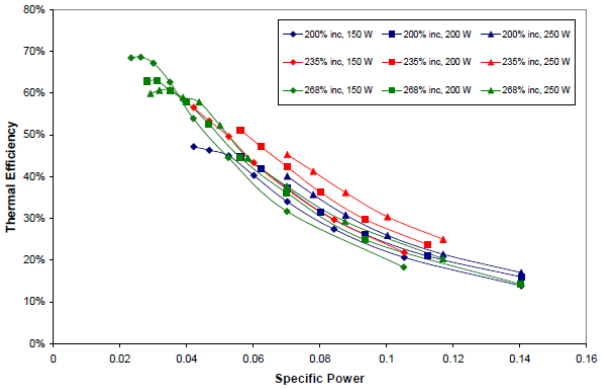

Figure 20. Thermal efficiency vs. specific power for various nozzles using 50% cold decomposed hydrazine.

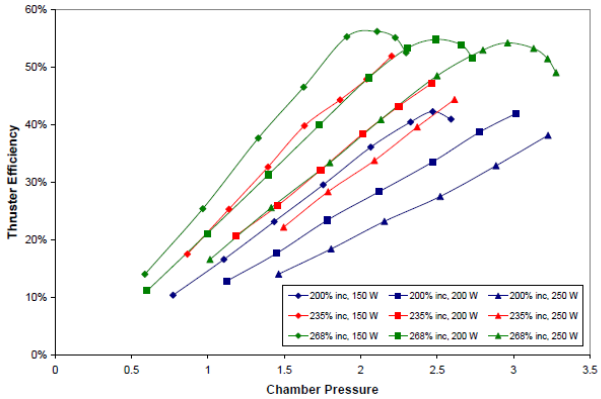

Figure 21. Thruster efficiency vs. normalized chamber pressure for various nozzles using 50% cold decomposed hydrazine.

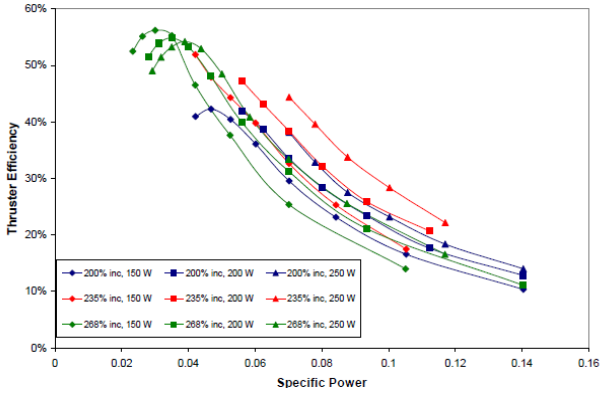

Figure 22. Thruster efficiency vs. normalized specific power for various nozzles using 50% cold decomposed hydrazine.

K. Simulated 50% Decomposed Hydrazine Propellant Results

Hydrazine is used in various operational propellant systems, which makes it a readily available propellant. The configuration of the MET used for simulated 50% decomposed hydrazine tests use the optimal antenna depth and injector size determined from the ammonia testing. The nozzle throat diameter was the only component

parameterized for optimization testing. The three nozzles used for this set of testing are the two largest nozzles used in ammonia testing and an additional nozzle that has a throat diameter 268% larger than the baseline nozzle used for ammonia testing. Coupling efficiency, thermal efficiency, thruster efficiency, and specific impulse are once again plotted against chamber pressure and specific power in order to asses the performance of the MET. Figs. 17–24 display the results of the simulated 50% decomposed hydrazine optimization testing. Again, the chamber pressure and specific power are normalized to the same testing configuration used to normalize the ammonia data.

The coupling efficiencies present in these results behave in the same manner as the ammonia data. In order to maintain maximum coupling efficiency when increasing power, an increase in mass flow is required. Thermal and thruster efficiencies of the simulated hydrazine also behave similarly to ammonia. A decrease in specific power results in an increase in these efficiencies. However, maximum thermal and thruster efficiencies do not appear to be attained. Nozzles with larger throat diameters need to be tested to verify these observations.

The specific impulse data are not as similar to the ammonia specific impulse results as the other performance evaluation values. Similar to the ammonia data, a minimum specific power value seems to exist. However, unlike ammonia, the maximum specific impulse is not attained with the nozzle configuration that achieves the lowest specific power. Instead the configuration using a nozzle with a throat area 235% larger than the baseline throat diameter is the highest performing nozzle. Once again as expected, specific impulse increases as input power increases.

It should be noted that the maximum thermal efficiency, maximum thruster efficiency, and maximum specific impulse observed for the simulated hydrazine tests are all less than the maxima observed from the ammonia tests, indicating that either the absolute simulated hydrazine maxima have yet to be attained or ammonia is a superior propellant. However, the maximum simulated 50% decomposed hydrazine specific impulse observed through this testing exceeds those reported in Ref. 4 for experimental maximum simulated 100% decomposed hydrazine specific impulse value by approximately 10%.

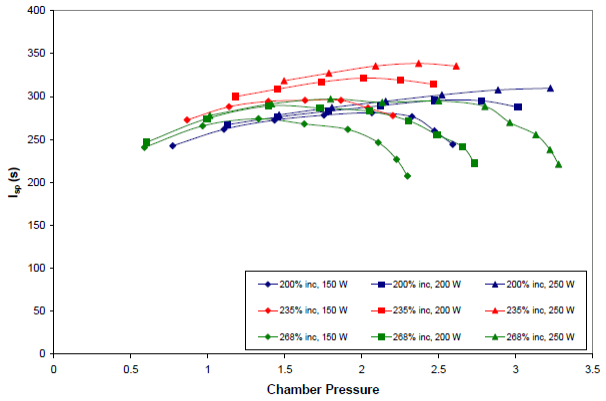

Figure 23. Specific impulse vs. normalized chamber pressure for various nozzles using 50% cold decomposed hydrazine.

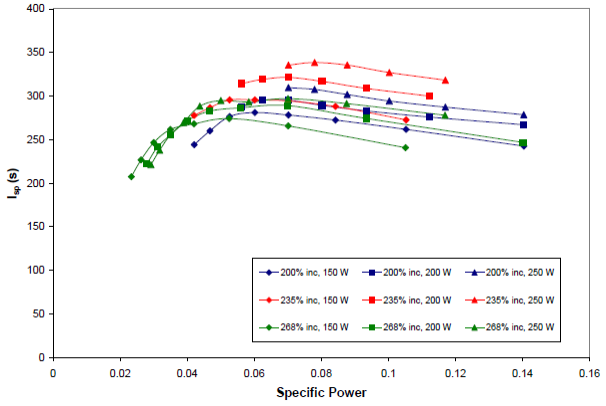

Figure 24. Specific impulse vs. normalized specific power for various nozzles using 50% cold decomposed hydrazine.

IV. Conclusions and Recommendations

The objective of the 8-GHz MET research presented here was to optimize the thruster configuration in order to achieve the best possible performance. The nitrogen testing showed that a one-piece thruster design cannot function over an extended period of time. Plasma created at the base of the thruster ultimately destroys the antenna and results in the inability of the MET to function. Antenna caps constructed from a material with a higher heat resistance could provide the needed protection for the antenna. Otherwise, it seems that a separation plate is required to operate the MET. The nitrogen testing also showed that a separation plate does not impede the performance of the thruster.

An optimized thruster configuration was determined when using ammonia propellant. The antenna depth is to be set at a 75% reduction of the baseline depth. The injector diameter size is to be the smallest possible without choking

the flow. The nozzle throat diameter is to be 235% larger than the baseline throat diameter. This configuration produced the highest specific impulse ever attained by any MET configuration using ammonia propellant, approximately 33% higher than the maximum specific impulse achieved by the 2.45-GHz MET. Significantly high efficiencies were achieved as well. However, because maximum thruster efficiency does not appear to have been reached, nozzles with larger throat diameters should be considered for testing. Higher power (400 W to 1000 W or higher) tests should be performed to obtain greater thruster performance. Finally, a nozzle constructed from a material with a lower thermal conductivity value than stainless steel should improve performance and be considered for testing.

Although specific impulse values attained through the simulated 50% decomposed hydrazine tests are greater than those reported in Ref. 4, simulated 50% decomposed hydrazine data showed that an optimal thruster configuration has yet to be determined. Nozzles with larger throat diameters may improve specific impulse and will likely improve thermal and thruster efficiencies. As with ammonia, a nozzle constructed from a lower thermal conductivity material as well as higher input power levels should also improve the performance of the thruster. Thruster optimization using simulated 80% decomposed hydrazine also must be conducted in order to determine the highest performing composition of simulated decomposed hydrazine products.

V. References

[1] Balaam, P., Maul, W., and Micci, M. M., "Characteristics of Free Floating Nitrogen and Helium Plasmas Generated in a Microwave Resonant Cavity," IEPC-88-099, 20th DGLR AIAA JSASS International Electric Propulsion Conference, Garmisch Partenkirchen, W. Germany, Oct 1988.

[2] Balaam, P. and Micci, M. "Investigation of Free Floating Nitrogen and Helium Plasmas generated in a microwave resonant cavity," AIAA-89-2380, 25th AIAA/ASME/SAE/ASEE Joint Propulsion Conference, Monterey, CA, July 1989.

[3] Clemens, D., *Performance Evaluation of a Low-Power Microwave Electrothermal Thruster*, Master of Science Thesis, Department of Aerospace Engineering, The Pennsylvania State University, 2004.

[4] Clemens, D., *Performance Evaluation of the Microwave Electrothermal Thruster Using Nitrogen, Simulated Hydrazine, and Ammonia*, Ph.D. Dissertation, Department of Aerospace Engineering, The Pennsylvania State University, 2008.

[5] Goovaerts, K., *Feasibility Studies of a 14.5 GHz, Low Power Microwave Electrothermal Thruster*, Master of Science Thesis, Department of Aerospace Engineering, The Pennsylvania State University, 2007.

[6] Kline, J., *Thrust Measurements of a Microwave Electrothermal Thruster*, Master of Science Thesis, Department of Aerospace Engineering, The Pennsylvania State University, 1996.

[7] Mueller, J., *Performance Evaluation and Operating Characteristics of a Waveguide Microwave Applicator for Space Propulsion Applications*, Ph.D. Dissertation, Department of Aerospace Engineering, The Pennsylvania State University, 1993.

[8] Nordling, D., *High-Frequency Low-Power Microwave Arcjet Thruster Development*, Master of Science Thesis, Department of Aerospace Engineering, The Pennsylvania State University, 1998.

[9] Roos, C., *Vertical-Deflection Thrust Stand Measurements of a Low Power Microwave Arcjet Thruster*, Master of Science Thesis, Department of Aerospace Engineering, The Pennsylvania State University, 2001.

[10] Souliez, F., *Low-Power Microwave Arcjet Spectroscopic Diagnostics and Performance Evaluation*, Master of Science Thesis, Department of Aerospace Engineering, The Pennsylvania State University, 1999.

[11] Souliez, F., Chianese, S., Dizac, G., and Micci, M., "Low Power Microwave Arcjet Testing: Plasma and Plume Diagnostics and Performance Evaluation," AIAA-99-2717, 35th AIAA/ASME/SAE/ASEE Joint Propulsion Conference, Los Angeles, CA, June 1999.

[12] Sullivan, D. J. and Micci, M., "The Effect of Molecular Propellants on the Performance of Resonant Cavity Electrothermal Thrusters," IEPC-91-034, 22nd DGLR AIAA JSASS International Electric Propulsion Conference, Viareggio, Italy, Oct 1991.

[13] Sullivan, D., *Development and Performance Characterization of a Microwave Electrothermal Thruster Prototype*, Ph.D. Dissertation, Department of Aerospace Engineering, The Pennsylvania State University, 1995.

[14] Welander, B., *Low-Power Microwave Arcjet Thruster Using Nitrogen Propellant*, Master of Science Thesis, Department of Aerospace Engineering, The Pennsylvania State University, 2004.

[15] Hill, P. and Peterson, C., *Mechanics and Thermodynamics of Propulsion*, 2nd Edition, Addison–Wesley Publishing Company, Inc., New York, 1992.